http://dx.doi.org/10.1590/0370-44672015690066

Gláucia Nascimento Queiroga
Professora Adjunta
Universidade Federal de Ouro Preto – UFOP
Escola de Minas
Departamento de Geologia
Ouro Preto – Minas Gerais – Brasil
glauciaqueiroga@yahoo.com.br

Bernhard Schulz
Professor
TU Bergakademie Freiberg - Institute of Mineralogy
Freiberg – Saxony - Germany
Bernhard.Schulz@mineral.tu-freiberg.de

Maximiliano de Souza Martins
Professor Adjunto
Universidade Federal de Ouro Preto – UFOP
Escola de Minas
Departamento de Geologia
Ouro Preto – Minas Gerais – Brasil
maximilianomartins@yahoo.com.br

Marco Paulo de Castro
Doutorando em Evoluçao Crustal e Recursos Naturais
Universidade Federal de Ouro Preto – UFOP
Escola de Minas
Departamento de Geologia
Ouro Preto – Minas Gerais - Brasil
marco_pcastro@yahoo.com

Antônio Carlos Pedrosa-Soares
Professor Titular
Universidade Federal de Minas Gerais – UFMG
Instituto de Geociências
Departamento de Geologia
Belo Horizonte – Minas Gerais – Brasil
pedrosa@igc.ufmg.br

Hanna Jordt-Evangelista
Professora Titular
Universidade Federal de Ouro Preto – UFOP
Escola de Minas
Departamento de Geologia
Ouro Preto – Minas Gerais – Brasil
hanna_jordt@yahoo.com.br

Ana Lúcia da Silva
Engenheira Geóloga
Universidade Federal de Ouro Preto – UFOP
Escola de Minas
Departamento de Geologia
Ouro Preto – Minas Gerais - Brasil
alucia.silva@hotmail.com

Thermobarometry and electron-microprobe Th-U-Pb monazite dating in garnet metapelites from the Capelinha Formation, Araçuaí Orogen, Brazil

Abstract

The Capelinha Formation (Macaúbas Group) consists of a lower quartzitic unit with metamafic intercalations and an upper metapelitic sequence. It occurs in a complex tectono-metamorphic sector of the Araçuaí orogen, where post-collisional collapse-related structures superimposed collisional structures. The garnet-bearing assemblages started crystallization in the collisional deformation stage that formed the main regional foliation around 570 Ma. Garnet porphyroblasts display a well-developed growth zonation of Fe-Mg-Ca-Mn and show, from core to rim, increasing almandine and pyrope contents in contrast with decreasing grossular and spessartine contents. Mineral relations and microstructures provide criteria for local equilibria and a structurally controlled application of geothermobarometers based on cation exchange and net transfer reactions. The P-T values calculated from cores to rims of garnets, aligned along clockwise trends, resulted in increasing temperatures (from 500 ºC up to 620 ºC) under decompression conditions (from 8.0 kbar to 4.5 kbar). The Th-U-Pb dating of homogeneous monazites by electron microprobe revealed a recrystallization period at around 490 – 480 Ma. These ages can be related to the tectono-thermal event associated with the gravitational collapse, constraining the youngest time limit for metamorphic processes in the Araçuaí orogen.

Keywords: Araçuaí orogen, Capelinha Formation, garnet metapelites, geothermobarometry, electron microprobe Th-U-Pb dating.

1. Introduction

The Capelinha Formation in the central-northern Araçuaí orogen comprises a thick metavolcano-sedimentary package cropping out in the vicinities of the homonymous town (Minas Gerais State, southeastern Brazil; Figure 1). It extensively occurs to the north of the Guanhães Block, between the Minas Novas Transpressive Corridor and the Chapada Acauã Shear Zone (Alkmim *et al.*, 2006), showing an E-W trending and south-verging fold system (Castro, 2014). Along this complex tectono-metamorphic sector of the Araçuaí orogen, post-collisional collapse-related structures (e.g., a crenulation cleavage to foliation associated with normal-sense shear zones and fold cascades) superimposed collisional structures (e.g., the main regional foliation associated with tight asymmetrical folds verging to SW) (Marshak *et al.*, 2006).

The upper metapelitic unit of the Capelinha Formation, focused on herein, extends along the north and south portions of the study area (Castro, 2014). It comprises (staurolite)-(kyanite)-garnet-mica schists with minor intercalations of carbonaceous schist, quartzite and calc-silicate rocks. Former studies on metamorphic features of the Capelinha metapelites took into account only the mineral assemblages and semi-quantitative analyses. Available age data on the metasedimentary rocks are restricted to the maximum depositional age of the basal metapsammitic unit (ca. 970 Ma; Castro *et al.*, 2013). Along these lines, this paper presents the chemical model (CHIME) Th-U-Pb monazite ages and geothermobarometric P-T paths from three samples of garnet-bearing micaschists from the upper unit of the Capelinha Formation, providing further time constraints for the evolution of the Araçuaí orogen.

2. Regional geology

The main rock units of the central-northern sector of the Araçuaí orogen includes three lithotectonic assemblages:

a) the Archean basement represented by the Guanhães complex;

b) the Tonian Capelinha Formation and,

c) the Cambrian Mangabeiras granitic suite (Figure 1).

The Archean Guanhães complex comprises an undivided assemblage of TTG (tonalite-trondhjemite-granodiorite) migmatitic orthogneisses and granitic bodies, commonly showing milonitic features, together with discontinuous lenses of banded iron formation and metavolcanic rocks (Noce *et al.*, 2007; Silveira-Braga *et al.*, 2015).

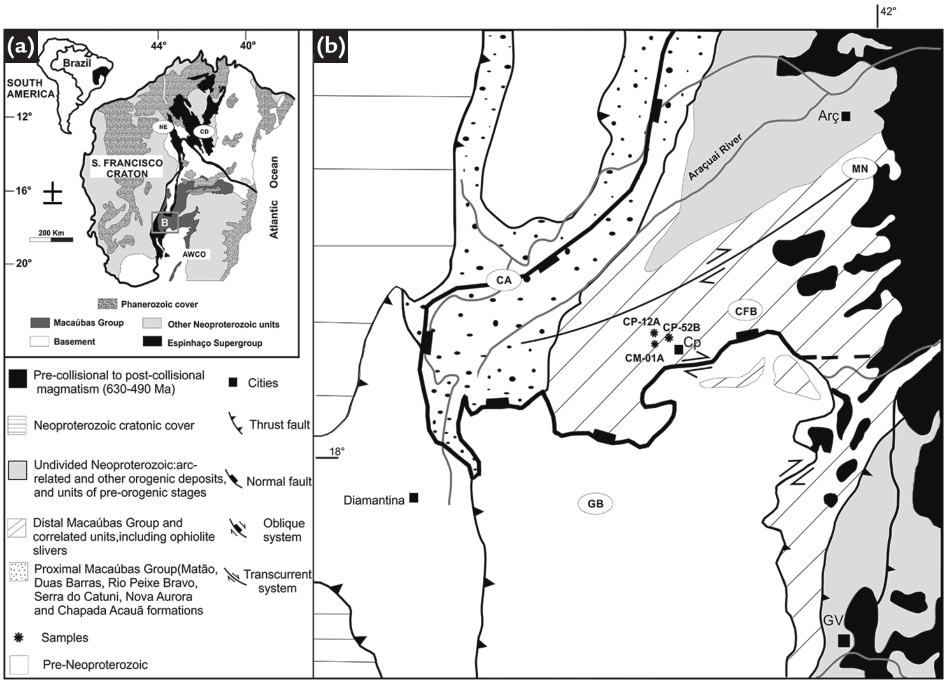

Figure 1
a) Geotectonic setting of the Araçuaí-West Congo orogen with a box indicating the location of the focused region.
b) Simplified geologic map of the Capelinha region highlighting the main lithotectonic assemblages. Capelinha Fold Belt (CFB), Guanhães Block (GB), Chapada Acauã Shear Zone (CA), Minas Novas Transpressive Corridor (MN). Asterisk refers to the collected samples.
Cities: Governador Valadares (GV), Capelinha (Cp), Araçuaí (Arç).

The Capelinha Formation, firstly defined by Grossi-Sad *et al.*, (1993) as a metasedimentary sequence of the upper Macaúbas Group, was recently redefined by Castro (2014) as a lateral equivalent to its pre-glacial units. It consists of a dominant metapsammitic basal sequence formed by mica schist, quartz schist and pure and/or micaceous quartzite, with lenses of metamafic rocks, and an upper metapelitic unit, mainly composed of peraluminous schists with garnet and/or staurolite and/or kyanite with minor contents of impure quartzite, carbonaceous schist and calc-silicate rocks. At the current stage of knowledge, the Capelinha Fold Belt (CFB) resembles an inverted and asymmetric fold belt, with the lower unit inserted in the core of kilometric anticlines. The structural assets indicate tectonic vergence to the south, against the Guanhães Block, where the detachment surface reveals itself as a normal fault with a dextral kinematic component that separates the Archean rocks of the Guanhães complex from the metasedimentary and metamafic rocks that belong to the Tonian Capelinha Formation (Figure 1). U-Pb LA-ICP-MS data from detrital zircon in three basal quartzites suggest that the maximum sedimentation age of the psamitic sequence is around 970 Ma (Castro *et al.*, 2013; Castro, 2014). The metamafic rocks, metamorphosed to amphibolite facies, have tholeiitic basalt protoliths with a dominant within-plate signature, Sm-Nd TDM model ages ranging from 1700 to 1400 Ma and slightly positive to negative epsilon Nd ($\varepsilon_{Nd\ (957\ Ma)}$ ranging from +0.21 to -3.64). U-Pb zircon ages for the amphibolites constraint magmat ic crystallization at 957 Ma and metamorphic recrystallization at around 569 Ma (Castro, 2014).

The Mangabeiras suite, representative of the G4 Supersuite from Pedrosa-Soares *et al.*, (2001, 2011), is composed of two-mica, biotite and muscovite-garnet leucogranite, free of the regional foliation. It encompasses three distinct bodies – Pedra Formosa, Córrego do Fogo and Barreiro. According to Pedrosa-Soares *et al.*, (2001, 2011), granite emplacement took place during the gravity collapse of the orogen, which lasted from 535 Ma to 490 Ma.

3. Analytical methods

Two-hundred quantitative analyses of garnet porphyroblasts and the coexisting biotite, muscovite and plagioclase from three garnet-bearing micaschists (samples CM01A, CP12A and CP52B; location presented in Figure 1), were performed with an electron microprobe JEOL JXA-8900 RL at the Institut für Werkstoffwissenschaft at Freiberg/Saxony, Germany. The electron beam was set at 15 kV, 20 nA, 2 µm and the common matrix ZAF corrections were applied. The elements analyzed were Si, Ti, Al, Fe, Mn, Mg Ca, Na and K, using wollastonite, rutile, garnet, hematite, bustamite, diopside, albite and orthoclase natural standards. Garnet and plagioclase were analyzed along transgranular profiles. Biotite and muscovite were characterized by few analyses from cores and rims.

Temperature and pressure conditions have been estimated using:

a) avPT (average P – T; Powell and Holland, 2008), an optimized method of Thermocalc 3.2 (Powell *et al.*, 1998);

b) garnet-biotite thermometer of Bhattacharya *et al.*, (1992) in combination with linearised calibration of the garnet-aluminosilicate-plagioclase (GASP) barometer, based on an internally consistent thermodynamic data set (Holland and Powell, 1990; Powell and Holland, 1994), with the activity models for garnet given by Ganguly *et al.*, (1996) and for plagioclase as proposed by Powell and Holland (1993) and,

c) conventional thermometry with calibrations by Thompson (1976), Holdoway and Lee (1977), Hodges and Spear (1982) and Perchuk and Lavrent`eva (1983).

In-situ analyses of Th, U, and Pb for the calculation of monazite model ages, as well as for Ca, Si, LREE and Y for the correction and evaluation of the mineral chemistry were carried out on the microprobe JEOL JXA8900 RL at Freiberg, using an acceleration voltage of 20 kV. The beam current was set 150 nA at a beam diameter of 5 µm. Madmon, a monazite from a pegmatite in Madagascar, acts as reference for monazite data and offline recalibration of ThO_2 (U-Pb-SHRIMP Madmon age of 496 ± 9 Ma, around 10 wt% ThO_2; Schulz *et al.*, 2007; Schulz and Schüssler, 2013). The calibration of PbO was realized on a crocoite standard, while U was calibrated with a U-metal. Orthophosphates of the Smithsonian Institution were used as standards for REE analysis (Jarosewich and Boatner, 1991; Donovan *et al.*, 2003). Prerequisites of the Th-U-Pb monazite dating method are (a) that monazite incorporates no common Pb when it crystallizes, (b) that no radiogenic Pb escaped, and (c) that no common Pb entered the monazite after the crystallization (Suzuki *et al.*, 1994; Montel *et al.*, 1996). The monazite chemical model ages were determined by following two approaches. First, for each single analysis, an age was calculated using the equations given by Montel *et al.*, (1996). The error resulting from counting statistics was typically on the order of ±20 to ±40 Ma (1σ) for Early Paleozoic ages. This error is reduced in Paleoproterozoic monazites due to their increased Pb contents. Using these apparent age data, weighted average ages for monazite populations in the samples were then calculated using Isoplot 3.0 (Ludwig, 2001) and are interpreted as the time of closure for the Th–U–Pb system of monazite during growth or recrystallization in the course of metamorphism. Second, the ages were determined using the ThO_2^*–PbO isochrone method (CHIME) of Montel *et al.*, (1996) and Suzuki *et al.*, (1994), where the age is calculated from the slope of the regression line in ThO_2^* vs PbO coordinates forced through zero. In all analyzed samples, the model ages obtained by the two different methods agree exceptionally well.

4. Petrography, mineral chemistry and geothermobarometry

As described in topic 2, the Capelinha Formation is composed of two different units – metapsammitic and metapelitic ones. The three studied metapelites, with low-variance mineral assemblages, were sampled northwest of the Capelinha city, close to the contact between both units (Figure 1). Large garnet porphyroblasts of up to 0.5 cm in length, fine – to medium grained heterogeneous fabric, and quartz bands are distinctive properties of the samples. The dark appearance leads to their abundance of biotite, forming mica clusters (Figure 2a). The metapelites main minerals are quartz, plagioclase, biotite, muscovite, garnet and kyanite (Figure 2b). Apatite, monazite, zircon and opaque minerals are the common accessories. Carbonate and sericite are the main alteration products of plagioclase.

The garnet-bearing micaschists display a well-developed foliation, Sn, commonly tightly folded (Figure 2A). The index minerals, like garnet and kyanite, mark the regional schistosity, being synkinematic in respect to the main deformation (Figure 2b). The garnet crystals are partially altered to biotite and enclose some biotite flakes, rounded quartz and opaque minerals. Small zircon and monazite grains are present in the foliated matrix, being related mostly to the quartz-feldspar portions. The S_{n+1} crenulation is marked by muscovite, biotite and chlorite and can be related to shallower crustal levels.

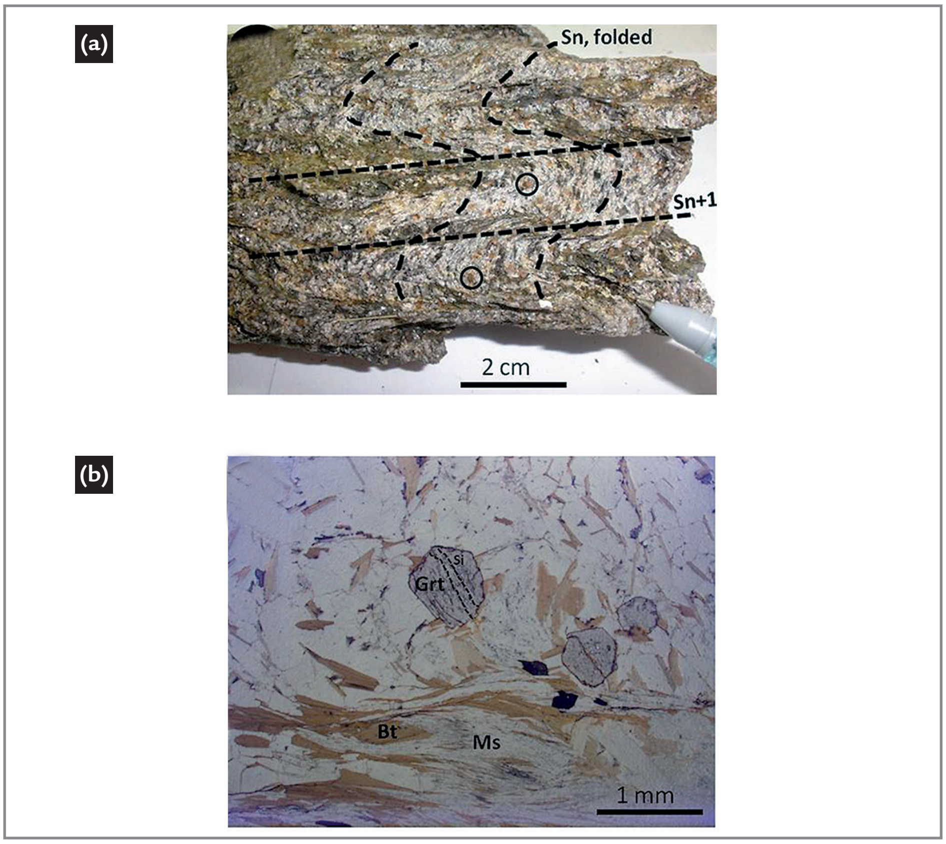

Figure 2
a) Dark garnet-bearing micaschist hand specimen – sample CP52B – showing the main foliation Sn folded (highlighted by the dotted lines). Some garnet porphyroblasts, with internal foliation Si, are marked using circles.
b) Microscope image of thin section CP52B exhibiting garnet (Grt) – biotite (Bt) – muscovite (Ms) assemblage.

A summary of the mineral chemical data from the studied samples is reported in Table 1 (complete data tables including the oxide compositions can be obtained from the first author). All the garnet porphyroblasts show well zoned profiles in all elements and having a distinctive rim-core-rim structure. The garnets are all almandine-dominated but comprise notable amounts of pyrope, grossular and spessartine. In the sample CM01A, for example, distinct and representative single analyses of the garnet zonation trend were selected, as labelled in the zonation profile of Figure 3.

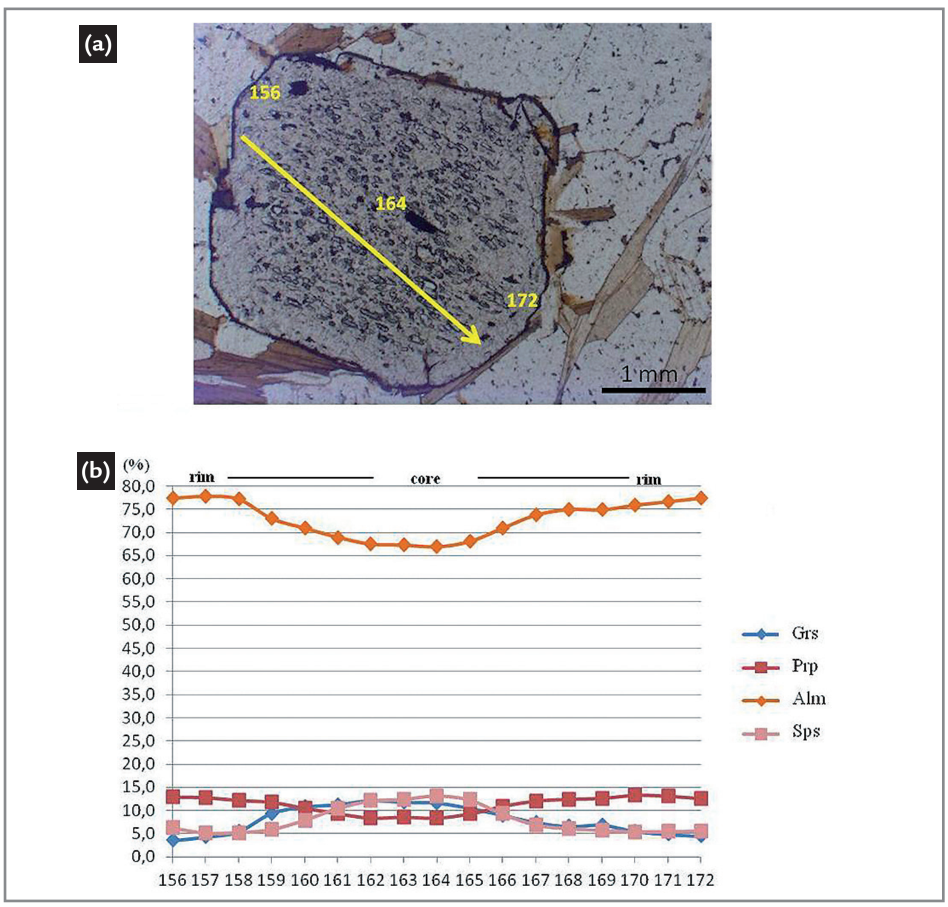

Figure 3
a) Garnet porphyroblast from the sample CM01A showing the analyzed profile (points 156 to 172; rim – core – rim).
b) Garnet zonation in Grossular (Grs) – Pyrope (Prp) – Almandine (Alm) – Spessartine (Sps) contents (% endmember) diagram.

Table 1
Summary of the electron microprobe analyses of garnet (Grt), biotite (Bt), muscovite (Ms) and plagioclase (Pl) in garnet-bearing micaschists, cations normalized to 12 O (garnet), 22 O (micas) and 8 O (plagioclase). Mineral analyses combined for geothermobarometric calculations are as follows: Sample CM01A: Grt164-Ms180-Bt174-Pl188; Grt172-Ms179-Bt175-Pl185; Sample CP12A: Grt88-Ms63--Bt94-Pl98; Grt93-Ms64-Bt96-Pl97; Sample CP52B: Grt66-Ms91-Bt88-Pl84; Grt74-Ms90-Bt89-Pl86. (Alm=almandine; Prp=pyrope; Sps=spessartine; Grs=grossular; An=anortite; c=core; r=rim).

	CM01A		CP12A		CP52B	
Grt	164-c	172-r	88-c	93-r	66-c	74-r
Si	3.027	3.020	3.029	2.996	3.002	2.999
Al	1.966	1.994	1.975	1.992	1.985	1.984
Fe	2.003	2.299	1.872	2.383	2.006	2.300
Mn	0.395	0.165	0.495	0.134	0.431	0.154
Mg	0.251	0.372	0.199	0.385	0.276	0.398
Ca	0.348	0.133	0.415	0.119	0.305	0.172
Tot.	7.990	7.983	7.985	8.009	8.005	8.007
Alm	66.8	77.4	62.8	78.9	66.5	76.0
Prp	8.4	12.5	6.7	12.8	9.1	13.2
Sps	13.2	5.6	16.6	4.4	14.3	5.1
Grs	11.6	4.5	13.9	3.9	10.1	5.7
Ms	180	179	63	64	91	90
Si	3.060	3.080	3.079	3.088	3.076	3.082
Ti	0.018	0.017	0.018	0.015	0.015	0.018
AlIV	0.940	0.920	0.921	0.912	0.924	0.918
AlVI	1.914	1.911	1.899	1.904	1.893	1.890
Fe	0.040	0.043	0.041	0.049	0.045	0.047
Mn	0.000	0.000	0.000	0.001	0.000	0.000
Mg	0.043	0.042	0.047	0.042	0.059	0.051
Na	0.314	0.283	0.216	0.233	0.238	0.266
K	0.641	0.664	0.760	0.721	0.736	0.716
Tot.	6.970	6.960	6.981	6.965	6.986	6.988
Bt	174	175	94	96	88	89
Si	2.736	2.750	2.733	2.761	2.741	2.747
Ti	0.084	0.091	0.089	0.083	0.086	0.085
AlIV	1.264	1.250	1.267	1.239	1.259	1.253
AlVI	0.438	0.421	0.422	0.420	0.427	0.417
Fe	1.158	1.145	1.117	1.112	1.128	1.142
Mn	0.004	0.001	0.002	0.002	0.006	0.001
Mg	1.227	1.228	1.317	1.316	1.242	1.255
Na	0.053	0.057	0.027	0.029	0.049	0.040
K	0.782	0.816	0.718	0.739	0.831	0.824
Tot.	7.746	7.759	7.692	7.701	7.769	7.764
XMg	0.422	0.426	0.447	0.449	0.431	0.433
Pl	188	185	98	97	84	86
Si	2.869	2.871	2.877	2.883	2.827	2.826
Al	1.117	1.112	1.114	1.109	1.131	1.138
Ca	0.141	0.137	0.138	0.134	0.154	0.149
Na	0.887	0.897	0.869	0.871	0.987	0.979
K	0.005	0.006	0.004	0.003	0.002	0.003
Tot.	5.019	5.023	5.002	5.000	5.101	5.095
An	13.7	13.2	13.7	13.3	13.5	13.2

The zonation profile in the largest garnets is characterized by the decreasing of spessartine (13 to 5.5 endmember%) and grossular (12.1 to 3.5%) components from the core to the rim (Figure 3). Pyrope has a minimum amount of 8.3 % in the core and increases to 13 % in the rim (Figure 3). Almandine has comparably high values and also increases from the core to the rim (66.8 to 77.4%) (Figure 3). The garnet chemical zonation, characterized by an increasing of Mg and Fe and a decreasing of Mn and Ca toward the borders, implies a prograde metamorphism. Plagioclase compositions range from An13 to An15 and the crystals can be classified as oligoclase. Biotite flakes are found mainly in the matrix and have similar X_{Mg} (Mg/Mg+Fe; 0.43 – 0.41). Muscovite X_{Mg} values range from 0.019 to 0.031.

Geothermobarometry based on mineral zonation of garnet-bearing assemblages revealed a clockwise P-T evolution with increasing temperature (500 ºC for cores to 627 ºC for rims using Thermocalc and 490 ºC for cores to 570 ºC for rims using the other geothermometers) and decompression (8.0 kbar for cores to 5.6 kbar for borders using conventional barometry and 6.7 kbar for cores to 4.4kbar for rims using Thermocalc) (Figure 4, Table 2). This corresponds to the low-to-intermediate amphibolite facies, with temperatures lower than the muscovite dehydration melting curve. The sample CP12A yielded the lowest P-T values for the garnet cores, showing that its crystallization started under greenschist facies conditions. The obtained P-T values are in agreement with the field metamorphic zoning observed in the Capelinha Fold Belt (Castro, 2014). The variation of the temperature values, given by Thermocalc and conventional thermometers, can be explained by the number of mineral phase considered for each method and also by the overall error (± 50ºC for the garnet-biotite pair, for example). For the pressure, the overall error is around 1.5 kbar.

Sample	THERMOCALC (Powell and Holland, 2008)		Conventional Thermobarometry Biotite + Garnet (Bhattacharya *et al.*, 1992) + GASP (Powell and Holland, 1993)		Conventional Thermometry			
					T76	HL77	HS82	PL83
	T (°C)	P(kbar)	T (°C)	P(kbar)	T (°C)	T (°C)	T (°C)	T (°C)
CM01A (core)	530 ± 23	6.2 ± 0.9	508	8.03	500	494	502	513
CM01A (rim)	627 ± 57	4.4 ± 1.5	560	6.32	554	542	544	553
CP12A (core)	501 ± 22	5.6 ± 0.8	466	7.74	458	457	462	482
CP12A (rim)	---	---	568	5.57	562	549	548	559
CP52B (core)	530 ± 25	6.7 ± 0.8	514	7.78	515	507	514	524
CP52B (rim)	580 ± 60	5.4 ± 1.3	570	7.32	566	553	563	562

Table 2
Geothermobarometric data for the garnet-bearing micaschists. T76 = Thompson (1976), HL77 = Hodges and Lee (1977), HS82 = Hodges and Spear (1982), PL83 = Perchuk and Lavrent'eva (1983).

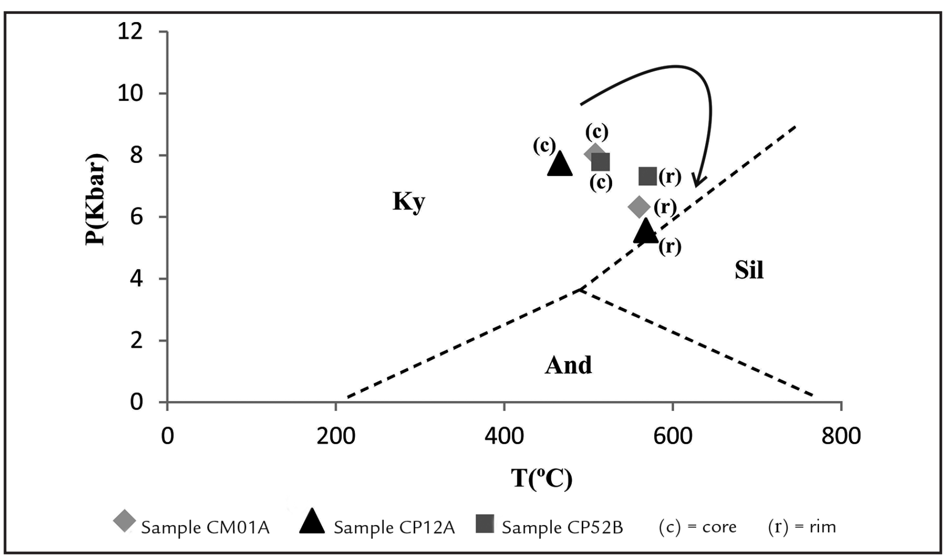

Figure 4
P-T data and P-T path segments from garnet-bearing micaschists. P-T results from the Grt-Bt thermometer of Bhattacharya *et al.*, (1992) and the GASP barometer (see text) applied to metapelite garnet assemblages. Stability fields for Kyanite (Ky), Andalusite (And) and Sillimanite (Sil) are given for overall orientation in P-T coordinates after Spear (1993).

5. Monazite dating by electron microprobe

The ThO_2*–PbO isochrone method (CHIME) was applied on three monazite-bearing micaschist samples. Results are listed in Table 3. The majority of the examined monazites are situated within the foliated matrix and have a maximal length of 100µm, allowing up to 6 single spot analyses in one grain (Figure 5). The detected monazites are generally homogeneous, rounded to weakly elongated and do not exhibit significant systematic inner zonation from older cores to younger rims.

Monazites of each sample do not stand out with distinct different compositions. The chemical analysis of 222 points in 101 different monazite grains shows contents of ThO_2 ranging from 2-8 wt%, UO_2 contents between 0.2 and 1.2 wt% while Y_2O_3 ranges from 0.7 to 2.4 wt% (Table 4).

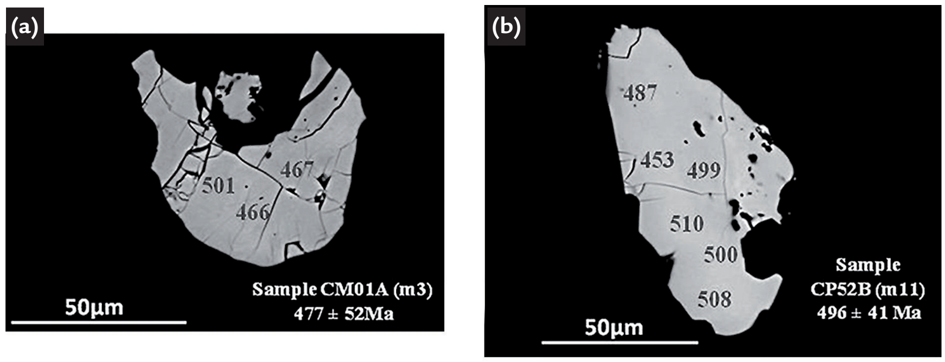

a) Monazite 3 (m3) of CM01A micaschist showing some cracks and 3 spot calculated ages.

b) Monazite 11 (m11) of CM52B sample with homogeneous shade of gray and 6 spot calculated ages.

Figure 5
Backscattered electron images (BSE) of monazites in garnet-bearing micaschists from Capelinha region. Numbers are EMP chemical ages from monazite single analyses. Weighted average Th-U-Pb CHIME ages with 2 sigma error are calculated from several analyses within a monazite grain. Locations of microprobe analyses are marked.

The micaschists display predominant Ordovician monazite ages along well-defined isochrones with weighted averages at 486 ± 10 Ma (CM01A), 478 ± 14 Ma (CP12A) and 487 ± 11 Ma (CP52B) (Figure 6a-c). As the weighted mean ages are base on single point data with consideration of a minimal error, in a statistical point of view the whole data set for each sample can be considered as a single population.

When the monazite age data is regarded in histograms one can recognize three sets of ages in all samples: a) an older maximum at 510 – 550 Ma, provided by a few grains (maybe older metamorphic relics?); b) a maximum of ages ranging at 470 – 510 Ma, the peak of monazite (re) crystallization, and c) the younger group of ages less than 470 Ma, interpreted here as due to minor lead loss (Figure 6d-f).

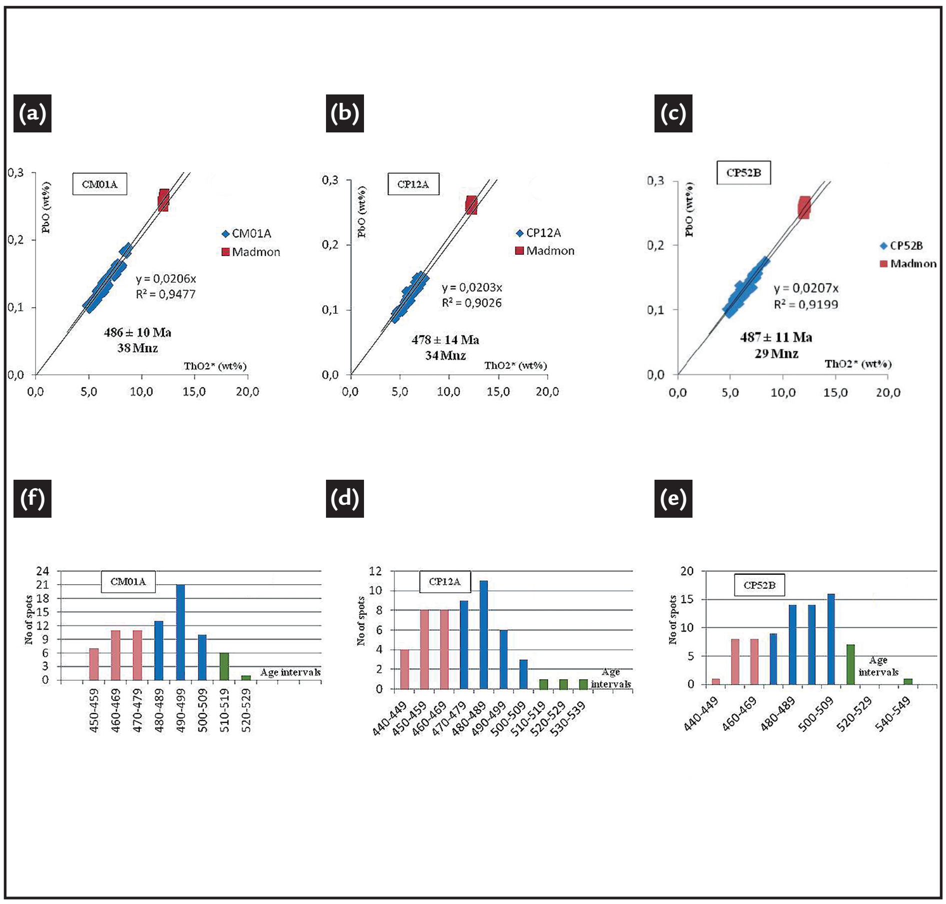

Figure 6
a – c) Th-U-Pb CHIME model ages in garnet-bearing micaschists from the Capelinha Formation. Total PbO vs. ThO_2* (wt.%); ThO_2* is ThO_2 + UO_2 equivalents expressed as ThO_2 after Suzuki *et al.*, (1994). Isochrones are calculated from regression forced through zero as proposed by Montel *et al.*, (1996). Isochrone ages match weighted average ages with error calculated according to Ludwig (2001). d-f) Histograms with the distribution of the different sets of monazite ages. Data from inhouse standard Madmon monazite (505 Ma) is shown for comparison.

Table 3
Electron microprobe analyses of metamorphic monazites from the three garnet-bearing micaschists from the Capelinha Formation.

Monazite	SiO_2	P_2O_5	CaO	Y_2O_3	La_2O_3	Ce_2O_3	Pr_2O_3	Sm_2O_3	Nd_2O_3	Gd_2O_3	ThO_2	UO_2	PbO	Total	Th	U	Pb	Th*	ThO_2*	Age	2σ
CM01A-m1	0.13	29.43	1.17	1.08	14.46	28.60	3.31	2.24	12.93	1.71	4.00	0.98	0.15	100.20	3.51	0.866	0.140	6.36	7.23	492	84
CM01A-m2-2	0.43	29.22	1.47	1.61	13.49	26.61	3.16	2.23	12.24	1.91	6.68	0.53	0.18	99.76	5.87	0.469	0.170	7.42	8.44	512	72
CM01A-m8-2	0.94	29.00	1.24	0.88	14.36	28.05	3.27	2.13	12.50	1.68	4.35	1.00	0.15	99.55	3.82	0.882	0.139	6.72	7.63	463	80
CM01A-m11	0.13	29.58	1.29	1.37	13.77	27.77	3.21	2.30	12.80	1.94	4.32	1.16	0.16	99.80	3.80	1.020	0.151	7.15	8.13	471	75
CM01A-m16-1	0.12	29.11	1.25	1.27	13.92	27.89	3.34	2.27	12.92	1.80	4.18	1.07	0.16	99.31	3.67	0.943	0.144	6.78	7.70	475	79
CM01A-m16-4	0.14	29.44	1.29	1.21	13.90	27.84	3.29	2.28	12.85	1.80	4.32	1.07	0.16	99.60	3.80	0.940	0.150	6.89	7.83	486	78
CM01A-m25	0.43	28.89	1.45	1.59	13.00	26.44	3.18	2.26	12.57	1.90	6.70	0.47	0.18	99.06	5.89	0.418	0.170	7.27	8.26	520	74
CM01A-m27-2	0.14	29.28	1.34	1.70	13.76	27.21	3.28	2.25	12.83	1.87	4.50	1.09	0.16	99.42	3.96	0.964	0.148	7.12	8.09	465	75
CM01A-m29	0.14	29.58	1.25	1.21	13.85	27.82	3.32	2.27	13.14	1.80	4.37	1.02	0.16	99.92	3.84	0.898	0.148	6.79	7.72	487	79
CM01A-m31	0.29	28.97	1.22	1.93	13.51	26.86	3.22	2.33	12.72	2.04	5.02	0.79	0.16	99.07	4.41	0.695	0.148	6.70	7.62	495	80
CM01A-m33-2	0.35	28.91	1.25	1.25	13.70	27.50	3.29	2.22	12.96	1.82	5.57	0.54	0.15	99.50	4.89	0.477	0.135	6.46	7.35	468	83
CM01A-m38-1	0.34	29.63	1.31	1.73	13.51	27.09	3.18	2.23	12.49	1.92	5.88	0.49	0.16	99.96	5.16	0.430	0.151	6.58	7.49	511	81
CM01A-m38-3	0.59	29.89	1.26	2.03	13.37	27.07	3.13	2.28	12.30	2.00	5.37	0.71	0.16	100.17	4.72	0.630	0.151	6.80	7.73	497	79
CP12A-m3	0.24	29.88	1.16	0.95	14.58	28.61	3.26	2.24	12.31	1.84	4.57	0.60	0.13	100.38	4.02	0.528	0.122	5.75	6.54	475	93
CP12A-m9	0.20	29.98	1.33	1.05	13.73	27.69	3.19	2.39	12.81	2.01	4.54	0.78	0.14	99.84	3.99	0.686	0.130	6.24	7.09	466	86
CP12A-m11-1	0.31	29.52	1.22	1.03	14.32	28.07	3.23	2.26	12.63	1.93	5.23	0.43	0.14	100.30	4.60	0.382	0.126	5.85	6.66	480	92
CP12A-m14-2	0.29	29.98	1.13	0.96	14.52	28.34	3.21	2.27	12.82	1.92	4.78	0.44	0.12	100.77	4.20	0.387	0.114	5.47	6.22	466	98
CP12A-m16-3	0.20	29.93	1.19	0.78	14.88	28.59	3.16	2.08	11.99	1.79	4.67	0.57	0.14	99.97	4.10	0.499	0.132	5.75	6.53	514	93
CP12A-m17	0.16	30.10	1.23	0.98	14.07	28.03	3.24	2.32	12.62	1.92	4.62	0.80	0.15	100.22	4.06	0.705	0.137	6.38	7.25	481	84
CP12A-m19-2	0.63	29.27	1.53	0.77	13.69	26.79	2.95	2.15	12.06	2.02	7.39	0.40	0.19	99.84	6.50	0.356	0.180	7.67	8.73	522	70
CP12A-m19-3	0.30	29.61	1.21	0.76	14.36	28.17	3.24	2.25	12.69	2.01	5.42	0.42	0.14	100.57	4.77	0.367	0.129	5.97	6.79	482	90
CP12A-m21-1	0.29	29.72	1.23	1.08	14.12	27.84	3.22	2.28	12.54	1.93	5.49	0.49	0.15	100.39	4.83	0.434	0.141	6.26	7.12	503	86
CP12A-m28	0.57	29.85	1.25	1.35	13.99	27.46	3.16	2.29	12.56	1.96	5.60	0.57	0.15	100.76	4.92	0.504	0.138	6.57	7.47	469	82
CP12A-m32-1	0.36	29.75	1.31	0.86	14.05	27.80	3.24	2.28	12.59	2.02	6.05	0.43	0.15	100.88	5.31	0.376	0.138	6.55	7.45	471	82
CP12A-m32-2	0.31	29.78	1.20	0.90	14.26	28.00	3.29	2.27	12.58	1.93	5.40	0.42	0.14	100.48	4.75	0.369	0.132	5.96	6.78	493	90
CP52B-m2-1	0.42	29.08	1.30	1.00	14.09	27.95	3.08	2.10	12.45	1.74	5.78	0.50	0.16	99.65	5.08	0.445	0.145	6.55	7.44	496	82
CP52B-m3-3	0.27	29.15	1.10	1.57	13.94	28.07	3.11	2.26	12.73	1.88	4.47	0.73	0.15	99.41	3.93	0.641	0.136	6.04	6.86	505	89
CP52B-m3-4	0.28	29.39	1.13	1.73	13.89	27.82	3.07	2.28	12.26	1.89	4.56	0.80	0.16	99.26	4.01	0.710	0.145	6.35	7.22	509	84
CP52B-m10	0.16	29.37	1.28	1.44	13.37	27.73	3.16	2.36	12.98	1.96	4.44	0.95	0.16	99.35	3.90	0.838	0.146	6.66	7.57	490	81
CP52B-m14-3	0.33	29.64	1.12	1.58	13.83	27.97	3.09	2.21	12.49	1.68	4.87	0.83	0.16	99.81	4.28	0.734	0.151	6.70	7.61	505	80
CP52B-m15-2	0.13	29.07	1.20	0.99	14.15	28.36	3.20	2.26	12.78	1.67	4.15	0.98	0.15	99.09	3.65	0.863	0.139	6.48	7.37	480	83
CP52B-m15-3	0.13	29.28	1.16	1.02	14.01	28.51	3.23	2.33	12.98	1.74	4.01	0.97	0.15	99.52	3.52	0.854	0.138	6.33	7.20	486	85
CP52B-m16-1	0.18	28.85	1.10	2.36	13.44	27.15	3.17	2.39	12.69	2.05	3.68	1.06	0.15	98.26	3.23	0.932	0.142	6.30	7.16	502	85
CP52B-m18	0.53	29.00	1.43	1.66	13.13	26.51	3.04	2.30	12.42	1.92	6.29	0.61	0.18	99.02	5.53	0.542	0.164	7.31	8.31	500	73
CP52B-m19	0.13	29.24	1.23	1.16	13.68	27.80	3.26	2.36	12.97	1.84	4.26	0.96	0.15	99.04	3.74	0.843	0.143	6.52	7.41	490	82
CP52B-m22-3	0.27	28.96	1.21	1.38	13.70	27.68	3.29	2.28	12.97	1.88	4.66	0.69	0.14	99.11	4.10	0.609	0.134	6.10	6.94	489	88
CP52B-m23-1	0.26	29.45	1.20	1.41	14.02	28.06	3.22	2.25	12.80	1.75	4.92	0.53	0.14	100.00	4.33	0.467	0.126	5.86	6.67	479	91
Madmon (ave)	3.01	25.03	0.16	0.96	8.11	25.26	3.89	4.56	15.85	2.22	10.78	0.36	0.26	100.45	9.47	0.31	0.24	10.51	11.95	505	10

Table 4
Monazite model ages, determined by electron microprobe, and a summary of the chemical composition of the analyzed grains for the three garnet-bearing micaschists.

Sample	Number of grains	Number of spots	Age (Ma)	ThO_2 contents (wt%)	UO_2 contents (wt%)	Y_2O_3 contents (wt%)
CM01A	38	84	486 ± 10	3.0 – 6.5	0.46 – 1.21	0.83 – 2.03
CP12A	34	55	478 ± 14	2.9 – 7.1	0.36 – 0.87	0.71 – 1.68
CP52B	29	83	487 ± 11	2.1 – 7.8	0.20 – 1.11	0.87 – 2.36

6. Conclusions

Temperature-pressure deformation trends were determined on the basis of numerous garnet profiles and are interpreted to reflect the local metamorphic evolution of the Capelinha region. Pervasively foliated, all the three pelitic samples show garnet porphyroblasts embedded in a fine to medium-grained muscovite-biotite-quartz-rich matrix. Kyanite is observed as the accompanying aluminosilicate. According to the microestructures, the large garnet crystals crystallized syndeformational and in course of the development of the regional foliation Sn, whose age was estimated at 569 ± 26 Ma (U-Pb LA-ICP-MS dating of titanite grains extracted from one amphibolite sample; Castro, 2014). All the analyzed garnets display prograde P-T zonations with uniformly decreasing spessartine and increasing pyrope and almandine contents from core to rim. Microstructurally-controlled geothermobarometry has been applied to the cores and inner rims of the garnet in the assemblages with biotite, muscovite and plagioclase. The thermobarometric results reflect their zonation trends and represent part of a clockwise evolution with increasing temperatures at decreasing pressures – from ca. 500 ºC up to 620 ºC and ca. 8.0kbar to 4.5kbar – within the kyanite stability field. This kind of pattern is very common in orogenic systems and the decompression could be due to erosion or tectonic denudation (Winter, 2001).

A significant number of monazite ages were calculated from the sampling spots. The backscattered electron imaging and analytical profiles revealed no distinct zonation graytones within the grains. Where the corresponding Th-U-Pb model ages are considered, there are no indications of distinguishable multiple monazite age generations within a sample. Almost similar isochrones in the ThO_2*/PbO plots were found in all of them. Actually, the monazites apparently resetted during a single event, as evidenced by the Ordovician ages (486 ± 10 Ma, 478 ± 14 Ma and 487 ± 11 Ma). This is the first time we found so young Ordovician ages for garnet-bearing micaschists from the Capelinha Formation. In fact, Cambrian ages have been systematically reported by some authors in the Guanhães complex and related granitoids. Fernandes (2001) presented the titanite age of ca.507 Ma (U-Pb TIMS) for the Statherian Borrachudos anorogenic granitoid. Piuzana et al., (2008) reported the titanite age of 506 ± 7 Ma for the trondhjemite gneiss of the Guanhães complex located south of the Capelinha region. Silva *et al*., (2011), for the biotite orthogneiss of the Guanhães complex situated at São João Evangelista town, presented the zircon age of 527 ± 45 Ma (U-Pb SHRIMP, inferior intercept). In the eastern part of the Araçuaí orogen, Richter (2015) has described similar Cambrian-Ordovician monazite ages on high-grade paragneisses, related to the back-arc basin, and on syn-collisional granitoids from Nova Venécia area.

Apparently, there is no link between the regional amphibolite facies thermal peak, dated at ca. 570 Ma in the Capelinha region (Castro, 2014) and the generation of monazite. Almost all of these youngest grains can be related to the tectonothermal event that occurred during the orogenic collapse. According to Alkmim *et al*., (2006), the collapse triggered igneous activity, due to decompression and partial melting of mid- and lower crustal levels, producing the free-foliation granitoids (520–490 Ma). The great volume of magma generated during the Cambrian-Ordovician time could be responsible for the monazite resetting/recrystallization, at lower temperature conditions than titanite and zircon and maybe connected with fluids, as reported in experimental studies by Seydoux-Guillaume *et al*., (2002).

7. Acknowledgments

The authors acknowledge financial support provided by FAPEMIG (project APQ04116) and UFOP (project PROPP number 03/2014 – Auxílio Financeiro ao Pesquisador) and G. Queiroga gratefully acknowledges grants provided by the DAAD – German and CAPES – Brazil organizations for a research stay at TU Bergakademie, Freiberg. We also thank the anonymous reviewers.

8. References

ALKMIM, F, F., MARSHAK, S., PEDROSA-SOARES, A.C., PERES, G.G., CRUZ, S.C.P., WHITTINGTON, A. Kinematic evolution of the Araçuaí-West Congo orogen in Brazil and Africa: Nutcracker tectonics during the Neoproterozoic assembly of Gondwana. ***Precambrian Research***, v. 149, p. 43-64, 2006.

BATTACHARYA, A., MOHANTY, L., MAJI, A., SEN, S.K., RAITH, M. Non-ideal mixing in the phogopite-annite boundary: constraints from experimental data on Mg-Fe partitioning and reformulation of the biotite-garnet geothermometer. ***Contributions to Mineralogy and Petrology***, v. 111, n. 1, p. 87-93, 1992.

CASTRO, M.P., QUEIROGA, G., MARTINS, M., DUSSIN, I.A., PEDROSA-SOARES, A.C., ALKMIM, F., CAVAGLIERI, H.M., ENDO, I. Caracterização lito-estrutural e geocronológica da Formação Capelinha na região homônima, Minas Gerais. In: SIMP. GEOL. SUDESTE, 13, 2013. Juiz de Fora. Resumos. Juiz de Fora: SBG, 2013, CD-ROM.

CASTRO, M.P. ***Caracterização geológica da Formação Capelinha como uma unidade basal do Grupo Macaúbas em sua área tipo, Minas Gerais.*** Ouro Preto: Departamento de Geologia, Universidade Federal de Ouro Preto, 2014. 114 f. (Dissertação de Mestrado).

DONOVAN, J.J., HANCHAR, J.M., PICOLLI, P.M., SCHRIER, M.D., BOATNER, L.A. & JAROSEWICH, E. A re-examination of the rare-earth element orthophosphate standards in use for electron-microprobe analysis. ***Canadian Mineralogist***, v. 41, p. 221-232, 2003.

FERNANDES, M.L.S. O Granito Borrachudos na região entre Guanhães e Dores de Guanhães, MG (Plutonito Morro do Urubu): gênese e evolução. Rio de Janeiro: Universidade Federal do Rio de Janeiro, 2001. 110 f. (Tese de Doutorado).

GANGULY, J., CHENG, W., TIRONE, M. Thermodynamics of aluminosilicate garnet solid solution: new experimental data, an optimized model, and thermometric applications. ***Contributions to Mineralogy and Petrology***, v. 126, n. 1-2, p. 137-151, 1996.

GROSSI-SAD, J.H., MOTTA, E., BAARS, F. Formação Capelinha: uma nova entidade litoestratigráfica do Grupo Macaúbas. In: SIMP. GEOL. MINAS GERAIS, 7, 1993. Belo Horizonte. Anais. Belo Horizonte: SBG, 1993. V.12, p. 30-33.

HODGES, K.V., SPEAR, F.S. Geothermometry, geobarometry and the Al2SiO5 triple point at Mt. Moosilauke, New Hampshire. ***American Mineralogist***, v. 67, p. 1118-1134, 1982.

HOLDOWAY, M.J., LEE, S.M. Fe-Mg cordierite stability in high-grade pelitic rocks based on experimental, theoretical and natural observations. ***Contributions to Mineralogy and Petrology***, v. 63, n. 2, p. 175-198, 1977.

HOLLAND, T.J.B. & POWELL, R. 1990. An enlarged and updated internally consistent thermodynamic dataset with uncertainties and correlations: the system K2O-Na_2O-CaO-MgO-MnO-FeO-Fe_2O_3-Al_2O_3-TiO_2-SiO_2-C-H_2-O_2. ***Journal of Metamorphic Geology***, v. 8, p. 89-124, 1990.

JAROSEWICH, E., BOATNER, L.A. Rare-earth element reference samples for electron microprobe analysis. ***Geostandards Newsletter***, v. 15, p. 397-399, 1991.

LUDWIG, K.R. Users manual for Isoplot/Ex rev. 2.49. A geochronological toolkit for Microsoft Excel. ***Berkeley Geochronology Center Special Publication***, v. 1a, p. 1-55, 2001.

MARSHAK S., ALKMIM F. F., WHITTINGTON A., PEDROSA-SOARES A. C. Extensional collapse in the Neoproterozoic Araçuaí orogen, eastern Brazil: A setting for reactivation of asymmetric crenulation cleavage. Journal of Structural Geology, v. 28, p. 129–147, 2006.

MONTEL. J.M., FOREST, S., VESCHAMBRE, M., NICOLLET, C., PROVOST, A. A fast, reliable, inexpensive in-situ dating technique: Electron microprobe ages on monazite. ***Chemical Geology***, v. 131,p. 37-53, 1996.

NOCE, C.M., PEDROSA-SOARES, A.C., SILVA, L.C., ALKMIM, F.F. O embasamento arqueano e paleoproterozóico do Orógeno Araçuaí. ***Geonomos***, v. 15, n. 1, p. 17-23, 2007.

PEDROSA-SOARES A.C., NOCE C.M., WIEDEMANN C.M., PINTO C.P. The Araçuaí–West Congo orogen in Brazil: An overview of a confined orogen formed during Gondwanland assembly. Precambrian Research, v. 110, p. 307-323, 2001.

PEDROSA-SOARES, A.C., DE CAMPOS, C.P., NOCE, C., SILVA, L.C., NOVO, T., RONCATO, R., MEDEIROS S., CASTAÑEDA C., QUEIROGA G., DANTAS E., DUSSIN I., ALKMIM F. Late Neoproterozoic–Cambrian granitic magmatism in the Araçuaí orogen (Brazil), the Eastern Brazilian Pegmatite Province and related mineral resources. ***Geological Society of London, Special Publications,*** v. 350, p. 25-51, 2011.

PERCHUK, L.L, LAVRENT'EVA, I.V. Experimental investigation of exchange equilibria in the system cordierite-garnet-biotite. In: SAXENA, S.K. (Ed.) ***Kinetics and Equilibrium in Mineral Reactions, Advances in Physical Geochemistry.*** New York: Springer-Verlag, 1983. p.199-239.

PIUZANA, D., CASTAÑEDA, C., NOCE, C.M., PEDROSA-SOARES, A.C., SILVA, L.C. Titanite crystal chemistry and U-Pb isotopic data: a petrogenetic indicator for Precambrian granitoid plutons of the Eastern Brazilian shield. Geonomos, v. 16, p. 29-36, 2008.

POWELL, R., HOLLAND, T.J.B. On the formulation of simple mixing models for complex phases. ***American Mineralogist***, v. 78, p. 1174-1180, 1993.

POWELL, R., HOLLAND, T.J.B. Optimal geothermometry and geobarometry. ***American Mineralogist***, v. 79, p. 120-133, 1994.

POWELL, R., HOLLAND, T.J.B. On thermobarometry. ***Journal of Metamorphic Geology,*** v. 26, p. 155-179, 2008.

POWELL, R., HOLLAND, T.J.B., WORLEY, B. Calculating phase diagrams involving solid solutions via non-linear equations, with examples using THERMOCALC. ***Journal of Metamorphic Geology***, v. 16, p. 577-588, 1998.

RICHTER, F. Sedimentation, metamorphism and granite generation in a back-arc region. Ouro Preto: Escola de Minas, Universidade Federal de Ouro Preto, 2015. 134 f. (Dissertação de Mestrado em Evolução Crustal e Recursos Naturais).

SCHULZ, B., SCHÜSSLER, U. Electron-microprobe Th-U-Pb monazite dating in Early-Paleozoic high-grade gneisses as a completion U-Pb isotopic ages (Wilson Terrane, Antarctica). Lithos, v. 175–176, p. 178–192, 2013.

SCHULZ, B., BRÄTZ, H., BOMBACH, K., KRENN, E. In-situ Th-Pb dating of monazite by 266 nm laser ablation and ICP-MS with a single collector, and its control by EMP analysis. Zeitsch. Angewandte Geologie, v. 35, p. 377-392, 2007.

SEYDOUX-GUILLAUME, A.M., PAQUETTE, J.L., WIEDENBECK, M., MONTEL, J.M., HEINRICH, W. Experimental resetting of the U–Th–Pb systems in monazite. Chemical Geology, v. 191, p. 165-181, 2002.

SILVA, L.C., PEDROSA-SOARES, A.C., ARMSTRONG, R., NOCE, C.M. Determinando a duração do período colisional do Orógeno Araçuaí com base em geocronologia U-Pb de alta resolução em zircão: uma contribuição para a história da amalgamação do Gondwana Ocidental. Geonomos, v. 19, n. 2, p. 180-197, 2011.

SILVEIRA-BRAGA, F.C., ROSIÉRE, C.A., QUEIROGA, G.N., ROLIM, V.K., SANTOS, J.O.S., MCNAUGHTON, N.J. The Statherian itabirite-bearing sequence from the Morro Escuro Ridge, Santa Maria de Itabira, Minas Gerais, Brazil. ***Journal of South American Earth Sciences,*** v. 58, p. 33-53, 2015.

SPEAR, F. Metamorphic phase equilibria and pressure-temperature-time paths. ***Mineralogical Society of America***, Series 1, 1993. 799p. (Monograph).

SUZUKI, K., ADACHI, M., KAJIZUKA, I. Electron microprobe observations of Pb diffusion in metamorphosed detrital monazites. ***Earth and Planetary Science Letters,*** v. 128, p. 391-405, 1994.

THOMPSON, A. B. Mineral reactions in pelitic rocks: II. Calculation of some P-T-X (Fe-Mg) phase relations. ***American Journal of Science***, v. 276, p. 401-454, 1976.

WINTER, O.D. ***An introduction to igneous and metamorphic petrology.*** New Jersey: Prentice Hall, 2001. 697p.

Received: 28 April 2015 - Accepted: 28 January 2016.